Kobe University Repository : Kernel

PDF issue: 2025-07-17

n-Type Carbon Nanotubes Doped by Cross-Linked Organic Superbase for Stable Thermoelectric Materials

Nishinaka, Mayuko
Wei, Qingshuo
Koshiba, Yasuko
Horike, Shohei

(Citation)
Energy Material Advances,5:0123

(Issue Date)
2024-01

(Resource Type)
journal article

(Version)
Version of Record

(Rights)
© 2024 Mayuko Nishinaka et al. Exclusive licensee Beijing Institute of Technology Press. No claim to original U.S. Government Works.
Creative Commons Attribution 4.0 International license

(URL)
https://hdl.handle.net/20.500.14094/0100491615

KOBE UNIVERSITY

Energy Material Advances
A SCIENCE PARTNER JOURNAL

RESEARCH ARTICLE

n-Type Carbon Nanotubes Doped by Cross-Linked Organic Superbase for Stable Thermoelectric Materials

Mayuko Nishinaka[1], Qingshuo Wei[2,3], Yasuko Koshiba[1,4], and Shohei Horike[1,2,4,5*]

[1]Department of Chemical Science and Engineering, Graduate School of Engineering, Kobe University, Kobe 657-8501, Japan. [2]Nanomaterials Research Institute, National Institute of Advanced Industrial Science and Technology (AIST), Tsukuba 305-8565, Japan. [3]Graduate School of Pure and Applied Science, University of Tsukuba, 1-1-1 Tennodai, Tsukuba 305-8577, Japan. [4]Research Center for Membrane and Film Technology, Kobe University, Kobe 657-8501, Japan. [5]Center for Environmental Management, Kobe University, Kobe 657-8501, Japan.

*Address correspondence to: horike@crystal.kobe-u.ac.jp

Citation: Nishinaka M, Wei Q, Koshiba Y, Horike S. n-Type Carbon Nanotubes Doped by Cross-Linked Organic Superbase for Stable Thermoelectric Materials. *Energy Mater. Adv.* 2024;5:Article 0123. https://doi.org/10.34133/energymatadv.0123

Submitted 1 June 2024
Accepted 9 August 2024
Published 6 September 2024

Copyright © 2024 Mayuko Nishinaka et al. Exclusive licensee Beijing Institute of Technology Press. No claim to original U.S. Government Works. Distributed under a Creative Commons Attribution License 4.0 (CC BY 4.0).

Carbon nanotubes (CNTs) are emerging as promising platforms for organic thermoelectric (TE) materials. However, the poor stability of n-doped states often presents a problem for the long-term operation of p–n junction TE modules. In this study, we synthesized a cross-linked organic superbase, 2TBD-C10, as a dopant to create n-type CNTs that are resistant to air, heat, and humidity. When comparing the stability of 2TBD-C10-doped CNTs with those doped by a conventional superbase (TBD), we found that the enhanced stability could be attributed to the unique molecular structure of 2TBD-C10. This structure aids in effective adsorption on the CNT surfaces through multiple points, reduces volatility because of increased molecular weight, and suppresses water adsorption owing to the presence of hydrophobic alkyl chains. The results of our study demonstrate that tailoring the primary molecular structures of dopants can remarkably improve the stability of doped states in CNTs. The stable n-type materials were integrated into all-CNT TE modules, achieving good-to-excellent performance (power output of approximately 35 μW from a temperature difference of approximately 65 °C), making them suitable for powering wireless sensors and green light-emitting diodes.

Introduction

The Internet of Things (IoT) is a crucial technology for optimizing energy consumption and time use, thereby aiding in the reduction of CO_2 emissions [1]. Given that trillions of sensors are likely to be utilized in future systems, conventional power supply methods (e.g., batteries) are impractical for powering such a vast number of sensors. Thermoelectric (TE) power generation is a promising alternative, enabling the automatic powering of sensors without maintenance by converting ubiquitous thermal energy into electricity [2,3].

The power factor (PF) is one of the performance indicators for TE materials, which can be expressed as

$$PF = S^2\sigma, \quad (1)$$

where S denotes the Seebeck coefficient and σ denotes the electrical conductivity [4]. The Seebeck coefficient is defined as the voltage output (ΔV) per temperature difference (ΔT) as follows:

$$S = -\frac{\Delta V}{\Delta T}. \quad (2)$$

Initially reliant on inorganic alloys, TE generators now explore organic alternatives, such as nanoscale carbon materials [5–8] and conducting polymers [9–12], because of their flexibility, low toxicity, resource abundance, and light-weight properties. Carbon nanotubes (CNTs) are especially promising candidates for a new class of TE materials because of their high electrical conductivity, Seebeck coefficient, and polarity (p- or n-type) tunability through chemical doping.

The ability to tune the polarity of CNTs is crucial for developing TE modules, because p- and n-type materials generate opposite potential gradients under a temperature difference, corresponding to Seebeck coefficients with opposite signs (positive for p-type and negative for n-type). Since the thermopower from a single TE material is limited, many p- and n-type materials need to be connected electrically in series and thermally in parallel to improve the voltage output to levels sufficient to activate DC-to-DC converters [13–16]. Therefore, both p- and n-type materials are necessary for developing practical TE modules.

The major carrier type of CNTs can be controlled by charge–transfer interactions with oxidizing (for p-type) and reducing (for n-type) chemicals attached to the CNT surfaces. The doped CNTs acquire positive and negative charges owing to electron withdrawal and injection, respectively [17–19], with counter ions adhering to the CNT surface to balance these charges [20].

Downloaded from https://spj.science.org at Kobe University on September 18, 2024

It is well recognized that CNTs suffer unintended p-type doping because of autoxidation in air, resulting in positive Seebeck coefficients [21,22]. Consequently, extensive efforts have been devoted to exploring n-type inducers for CNTs. For instance, alkali metals [23], amines [24,25], phosphines [26], and supramolecular salts [27] have been suggested as feasible reductants.

Meanwhile, the stability of the n-doped states must be recognized as one of the most crucial issues for achieving fully organic TE modules. Since TE modules will be placed on heat sources, thermal stability is essential for ensuring long-term operation. We recently identified a bicyclic-ring organic superbase, 1,5,7-triazabicyclo[4.4.0]dec-5-ene (TBD) (Fig. 1), as an efficient molecule that can induce n-type polarity in CNTs with outstanding thermal stability, lasting for more than 6 months at 100 °C in air [28]. This high stability was attributed to the excellent adsorption ability of the TBD cation onto the CNT surfaces because of its rigid, planar molecular shape, which creates an energetically favored charge transfer complex, as revealed by quantum calculations [29]. This was further evidenced by comparisons with the poor stability of n-type CNTs doped with an acyclic organic superbase that shares the guanidine backbone with TBD. Although the thermal stability of TBD-doped CNTs is remarkable, the gradual decrease in electrical conductivity and increase in the negative Seebeck coefficient indicate partial dedoping over long-term incubation [28,29]. Therefore, n-type dopants that can retain the TE properties of CNTs for extended periods should be explored to ensure stable power generation. Additionally, it is important to investigate the stability of n-doped CNTs stored at room temperature and/or in humid conditions.

In this study, we synthesized a TBD derivative, where 2 TBD molecules are cross-linked by normal decane (2TBD-C10; Fig. 1), as an n-type dopant for CNTs with improved stability. This molecule was selected for the following reasons. (a) TBD has good adsorption ability owing to its rigid, planar molecular shape, as revealed previously by quantum calculations [29]. Therefore, each TBD unit can donate an electron to the CNTs, and the resulting TBD cations would attach to the CNTs with high affinity. This multipoint adsorption would help to suppress dopant detachment. (b) The increased molecular weight of 2TBD-C10 may reduce its volatility. According to the Hertz–Knudsen–Langmuir equation, molecules with a higher molecular weight have a lower saturation vapor pressure [30]. (c) Introducing a hydrophobic alkyl chain in the dopant molecule would hinder water molecules from approaching the CNT surfaces, potentially decreasing the effects of dedoping or carrier trapping by water molecules in humid conditions.

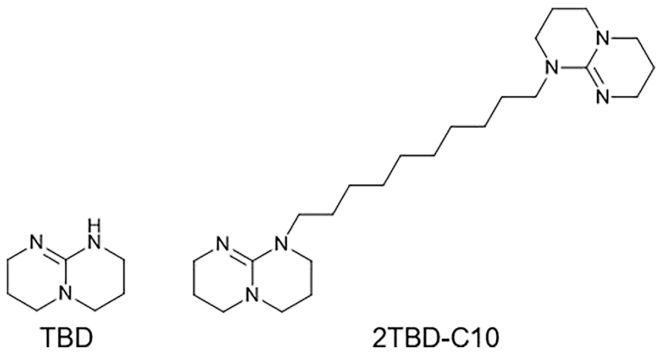

Fig. 1. Molecular structures of TBD and 2TBD-C10.

Our comprehensive analysis, including tests of the retention ability of TE properties in doped CNTs under various conditions, demonstrates that customizing the primary molecular structure of the dopant plays a pivotal role in improving the stability of doped states in CNTs. Furthermore, we demonstrate all-CNT TE modules—which can be used for powering IoT sensors—by combining the n-doped CNT films with p-type CNT films.

Materials and Methods

Chemicals and materials

The chemicals and materials used in this study, along with their suppliers and purities, are listed in Table S1.

Synthesis and characterization of 2TBD-C10

2TBD-C10 was synthesized according to the procedure reported by Nakayama et al. [31]. A flask containing 7.35 mmol of NaH was rinsed with hexane to remove the paraffin residue. After drying under Ar gas flow, 50 ml of dehydrated tetrahydrofuran and 5.39 mmol of TBD were added. After stirring the mixture at room temperature for 4 h under continuous Ar gas flow, 2.45 mmol of 1,10-dibromodecane was added, followed by stirring at room temperature overnight. The resulting pale-yellow solution was vacuum-filtered to remove precipitates. The filtrate was refluxed, and the waxy compound obtained was decanted with 5 ml of hexane 3 times. The hexane fraction was dried at 50 °C in vacuo. 2TBD-C10 was collected as a pale-yellow waxy solid (yield: 69%).

The synthesized 2TBD-C10 was characterized by nuclear magnetic resonance (NMR) and mass spectrometry (MS). NMR spectra of a deuterated chloroform solution of 2TBD-C10 were recorded using a JNM-ECZS spectrometer (JEOL). MS of a chloroform solution of 2TBD-C10 was performed using a JMS-T100LP AccuTOF LC-Plus (electrospray ionization) with MS-5414DART (JEOL). DART mass: $m/z = 417.37$ $[M+H]^+$ (calculated for $C_{24}H_{45}N_6H^+$ $[M+H]^+ = 417.37$).

The thermal properties of 2TBD-C10 were measured by thermogravimetry (TG) and differential scanning calorimetry (DSC). For TG measurements, the sample was loaded into a cylindrical Al_2O_3 open crucible and set on the thermobalance of the TG setup (HV-STA2500 Regulus, NETZSCH Japan) with an empty reference crucible. The TG curve was recorded while heating the sample at a rate of 10 °C min^{-1} under N_2 flow (0.15 l min^{-1}). For DSC measurements, the sample was loaded into a cylindrical Al crucible, closed with a lid, and placed in the instrument (DSC8230, Rigaku) with an empty reference crucible. The DSC curve was recorded under N_2 flow within the temperature range of −50 and +230 °C. The heating and cooling rates were set to 10 °C min^{-1}.

Formation and doping of self-standing CNT films

Self-standing CNT films with a diameter of approximately 70 mm and thickness of approximately 30 μm were prepared according to a procedure reported elsewhere [28,29]. Briefly, an aqueous solution (90 ml) of Brij L4 nonionic surfactant was prepared at a concentration of 1.3 mg ml^{-1}. CNT powder (113 mg) was roughly dispersed in the solution using an ultrasonic homogenizer (Q500, QSONICA) in an ice bath. The CNT dispersion was vacuum-filtered through a polytetrafluoroethylene membrane (H020A090C, ADVANTEC) to form a CNT film

Downloaded from https://spj.science.org at Kobe University on September 18, 2024

on the membrane. The CNT film was rinsed with water and acetone after being peeled from the filter. The obtained self-standing film was dried in air overnight and cut into 10 × 15 mm pieces prior to doping and characterization. TBD and 2TBD-C10 were dissolved in separate solvents [acetone, *N*,*N*-dimethylformamide (DMF), or ethanol] at a concentration of 71.8 mM (corresponding to 10 mg ml^{-1} for the TBD solution, which was previously found to be sufficient for the n-type doping of CNTs [28]). Doping was conducted by immersing the films in the dopant solutions in 30-ml-sized screw vials and then drying in vacuo for more than 30 min.

Characterization of CNT films

Electrical and spectroscopic characterizations of CNT films were conducted at room temperature in air. The thickness of the CNT films was measured using the differential transformer principle with a VL-5 apparatus (Mitutoyo). For Seebeck measurements, a temperature difference was applied to the CNT film in the in-plane direction using 2 Peltier modules (VPE20-30S, VICS). Two R-type thermocouples were attached to the CNT films to simultaneously measure the temperature difference and output voltage using a data logger (LR8400, HIOKI). The Seebeck coefficient (S) was calculated from the slope of thermopower ($-\Delta V$) versus the temperature difference (ΔT) according to Eq. 2.

The electrical conductivity of the CNT films was measured by the 4-probe method with a resistivity meter (Loresta-GX MCP-T700, Nittoseiko Analytech). The stability of the TE properties in hot and humid environments was investigated as follows. For the thermal stability, the films were stored in an incubator (ETTAS OFP-600V, AS ONE) at 100 °C in air. For the humidity stability, the films were stored in a glove box (AS-600PC, AS ONE) at room temperature, with the humidity maintained above 80% by placing a beaker filled with deionized water in the chamber. The TE properties were measured in ambient air after removing the specimens from the incubator or glove box. Raman spectra were recorded using a Raman spectrometer (NRS-7100, JASCO) with a 532-nm excitation laser. Scanning electron microscopy (SEM) was conducted using a commercial field-emission scanning electron microscope (JSM-IT800HL, JEOL).

Fabrication and characterization of all-CNT TE module

An all-CNT TE module was fabricated according to a procedure similar to that reported in our previous paper [28]. First, the CNT films, both before and after doping, were pressed using a hydrostatic pressurizer at 3 MPa and room temperature. This step ensured that the film shape remained unchanged during the subsequent lamination process. Next, both n- and p-type CNT films were cut into squares with dimensions of 2.2 × 2.2 cm using a precision film cutter (NOGAMIGIKEN Co. Ltd.). The p-type CNT films, insulating polyimide (PI) films (1.8 × 2.3 cm), and n-type CNT films were subsequently stacked and laminated at 50 °C and 3 MPa using a hydrostatic pressurizer with hot plates (AH-1TC, AS ONE).

The contact resistance was measured using the transfer length method. The n-type CNT film was first cut into strips measuring 0.3 × 10 cm. Then, p-type CNT films with dimensions of 0.3 × 0.5 cm were laminated onto the surface of the n-type CNT film. The overlapping area was 0.3 × 0.3 cm, and the distance between the p-type CNT films varied from 0.2 to 4.4 cm. A 0.3 × 0.3 cm Au plate was placed on the surface as the electrode for resistance measurements.

Results

Thermal analysis of 2TBD-C10

2TBD-C10 was synthesized according to the procedure reported by Nakayama et al. [31]. The NMR spectrum is shown in Fig. S1. The thermal properties of 2TBD-C10 were characterized by TG and DSC. The TG curve, shown in Fig. 2A, confirms the relatively high degradation temperature of 2TBD-C10, with a 5% weight loss temperature of 314 °C. This observation aligns with the report by Nakayama et al. [31]. Meanwhile, the DSC curve, shown in Fig. 2B, indicates a melting point of 22 °C and supercooling behavior with a solidification temperature of −48 °C. Considering the baseline shift at approximately 150 °C and the difference between the first- and second-cycle data (Fig. S2), the degradation of 2TBD-C10 occurs above 150 °C. Based on these observations, we tested the thermal stability of the 2TBD-C10-doped CNTs at 100 °C.

TE characterization of 2TBD-C10-doped n-type CNTs

The as-prepared CNT films had good electrical conductivity (approximately 1,300 S cm^{-1}) and a Seebeck coefficient of approximately +46 μV K^{-1}. The positive sign of the Seebeck coefficient, determined from the slopes of the $-\Delta V$ versus ΔT plots shown in Fig. 3A and B, indicates the p-type polarity of the as-prepared CNT films because of autoxidation in air [21,22]. Doping with 2TBD-C10 and TBD (for comparison) was conducted by immersing the CNT films in acetone solutions with a concentration of 71.8 mM at approximately 25 °C for 5 min and drying under vacuum. The conversion of the Seebeck coefficient from positive to negative (approximately −20 μV K^{-1}) upon doping with 2TBD-C10 and TBD (Fig. 3A and B, respectively) indicates the alteration of the major carrier species of CNTs from holes to electrons [32]. Doping with these bases increased the electrical conductivity of the CNT films to 1,500 and 2,130 S cm^{-1} for 2TBD-C10 and TBD, respectively. Considering the increased conductivity and decreased absolute value of the Seebeck coefficient, along with the typical trade-off relation between the conductivity and Seebeck coefficient according to the carrier density [33], electrons were injected into the CNTs with a higher density than that of the original holes introduced by oxygen impurities in air. Furthermore, the higher conductivity of the TBD-doped CNT films indicates that a higher electron density is achieved by doping with TBD than with 2TBD-C10.

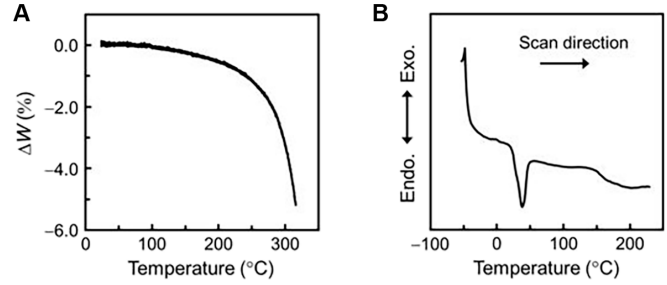

Fig. 2. Thermal analyses of 2TBD-C10. (A) TG and (B) first-cycle DSC data of 2TBD-C10 under N_2 gas flow.

Downloaded from https://spj.science.org at Kobe University on September 18, 2024

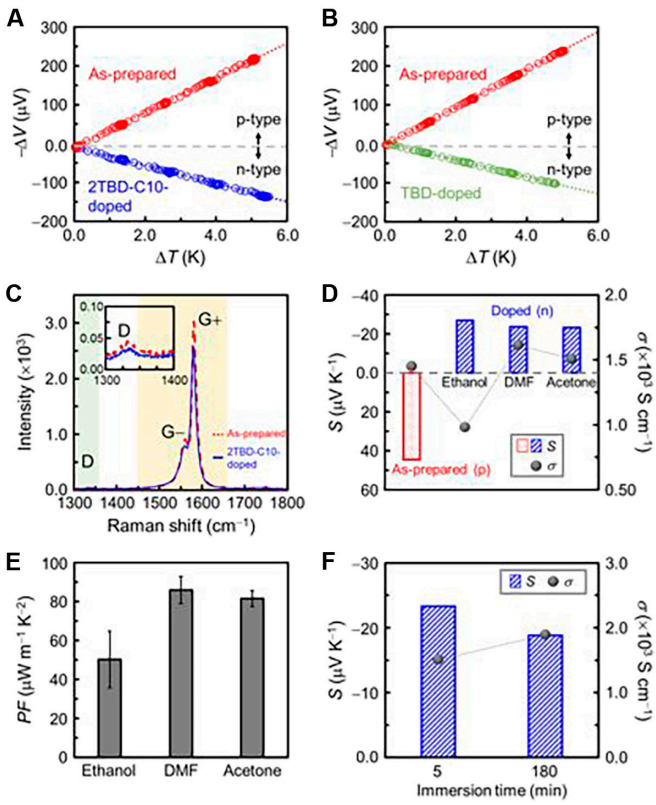

Fig. 3. Thermoelectric and spectroscopic characterization of n-doped CNT films. Plots of thermopower ($-\Delta V$) against the supplied temperature difference (ΔT) of CNT films to extract the Seebeck coefficients (S) for (A) as-prepared and 2TBD-C10-doped and (B) as-prepared and TBD-doped CNTs. (C) Raman spectra of as-prepared and 2TBD-C10-doped CNT films. The inset shows an enlarged view of the D bands. Solvent dependencies of (D) Seebeck coefficient and electrical conductivity (σ) and (E) power factor (PF) of 2TBD-C10-doped CNT films by immersing the dopant solutions for 5 min. (F) Immersion-time dependency of the Seebeck coefficient and electrical conductivity of 2TBD-doped CNT films.

The Raman spectra of the CNTs before and after 2TBD-C10 doping are compared in Fig. 3C to reveal structural changes in the CNTs. All CNT samples showed typical G band (1,550 to 1,580 cm^{-1}) and D band (approximately 1,330 cm^{-1}) features. The G^+/D and G^-/D ratios (an indicator of sp^2 integrity) and peak positions remained unchanged after doping, as listed in Table S2. Therefore, 2TBD-C10 doping did not cause severe damage to the sp^2 framework of the CNTs. It is likely that the conjugate acid of 2TBD-C10 is physisorbed onto the CNT surface as a result of charge transfer.

The n-type doping of CNTs using amine compounds is expected to occur through the donation of lone-pair electrons on nitrogen atoms to CNTs ($n \rightarrow \pi^*$ interaction) [28,34]. The efficiency of this charge transfer process can be influenced by solvents, akin to considerations in organic synthesis [35,36]. To investigate this, the TE properties of 2TBD-C10-doped CNT films were compared based on the solvent used for doping. Figure 3D illustrates the variations in the TE properties of 2TBD-C10-doped CNT films mediated by polar aprotic solvents (acetone and DMF) and a polar protic solvent (ethanol). While all cases demonstrated the conversion of CNT polarity to n-type, as indicated by the negative Seebeck coefficients, the CNT films doped in ethanol had electrical conductivities of less than 1,000 S cm^{-1}, whereas those doped in DMF and acetone exhibited relatively high values (1,500 to 1,600 S cm^{-1}). Additionally, the CNTs doped in DMF and acetone showed lower absolute values of the Seebeck coefficients than those doped in ethanol. Considering the typical trade-off relation between the conductivity and Seebeck coefficient according to the carrier density [33], 2TBD-C10 exhibits stronger reducing ability for CNTs in polar aprotic solvents than in protic ones. In protic solvents, the transfer of lone-pair electrons may be kinetically hindered because of hydrogen bonding between the nitrogen atoms of 2TBD-C10 and the acidic hydrogen atoms of the solvents [37]. These observations align with data reported in our previous paper using TBD as a dopant [28]. Figure 3E depicts the solvent dependence of the power factor (PF). CNTs doped in the polar aprotic solvents demonstrated higher PF values (82–86 μW m^{-1} K^{-2}) than those doped in the polar protic solvent (50 μW m^{-1} K^{-2}). These comparisons demonstrate that the selection of solvent is essential for doping with 2TBD-C10.

The immersion-time dependency of the TE properties of 2TBD-C10-doped CNTs confirmed that the electron transfer reaction between 2TBD-C10 and CNTs could be completed in a fairly short time, as shown in Fig. 3F. CNT films immersed in the acetone solution of 2TBD-C10 for 3 h exhibited higher electrical conductivity (1,710 S cm^{-1}) and a lower absolute value of the Seebeck coefficient (−21 μV K^{-1}) compared to those immersed for 5 min (1,500 cm^{-1} and −23 μV K^{-1}), although the differences were not remarkable. This indicates that electron transfer in the solution is almost completed within 5 min. Based on these experimental results and considerations, the subsequent doping process for stability tests was conducted by immersing the CNT films in the acetone solution of 2TBD-C10 (or TBD) for 5 min.

Thermal stability of the doped CNT films

Although the TBD-doped CNTs retained their n-type polarity for an extended period at 100 °C in air, partial dedoping was observed, as indicated by the decrease in electrical conductivity and increase in the absolute value of the negative Seebeck coefficient over time (Fig. 4A). This aligns with our previous report [28]. Specifically, the absolute value of S increased from −21 to −35 μV K^{-1} and σ decreased from 2,130 to 750 S cm^{-1} (approximately 65% decrease) after incubation at 100 °C in air for 3,600 h.

Surprisingly, the 2TBD-C10-doped CNT films exhibited a decrease in the absolute value of the negative S (from −23 to −18 μV K^{-1}) and an increase in σ (from 1,500 to 2,630 S cm^{-1}) after incubation at 100 °C in air for 24 h, as shown in Fig. 4B, indicating that additional electron doping occurred because of heating. This doping progression can be attributed to the structural rearrangement of 2TBD-C10 on the CNT surfaces. The high degree of conformational freedom of the cross-linking decyl group and the relatively large molecular size of 2TBD-C10 suggest that unreacted TBD components may still be present after the solution-mediated doping process. The thermal energy supplied during incubation would facilitate the structural rearrangement of 2TBD-C10, allowing the unreacted TBD components to react with the CNTs and contribute to additional electron injections. This doping progression is a notable difference from TBD-doped CNTs, stemming from the structural flexibility of 2TBD-C10.

Once the doping progression reached saturation, the 2TBD-C10-doped CNT films showed a slight decrease in σ and increase in the absolute value of negative S, reflecting partial dedoping. However, these changes almost plateaued after approximately 1,600 h of incubation. Furthermore, the depletion of the TE

Downloaded from https://spj.science.org at Kobe University on September 18, 2024

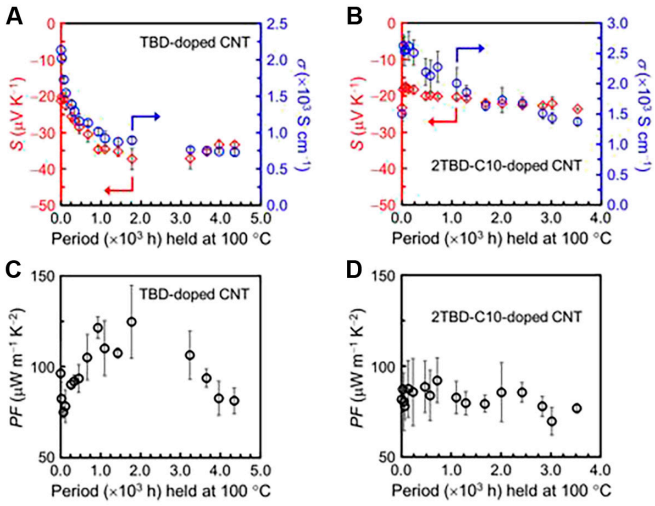

Fig. 4. Thermal stability of n-doped CNT films. Changes in (A and B) Seebeck coefficient (S) and electrical conductivity (σ) and (C and D) power factor (PF) of n-doped CNT films during incubation at 100 °C in air: (A and C) TBD-doped and (B and D) 2TBD-C10-doped CNT films.

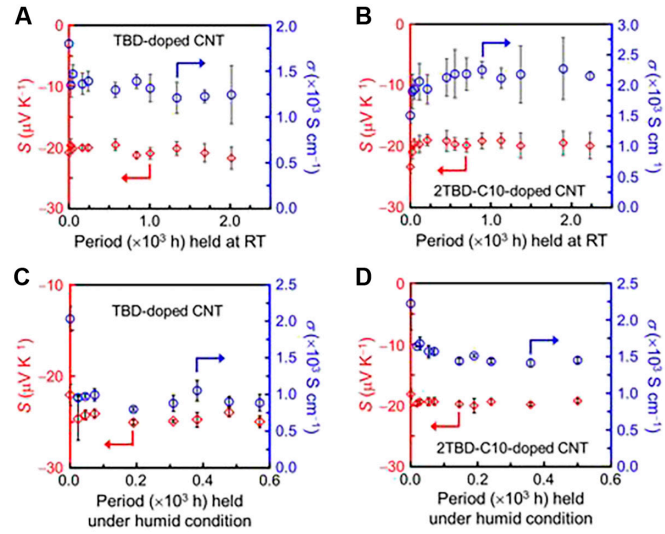

Fig. 5. Stability of n-doped CNT films in air and under humid conditions. Changes in Seebeck coefficient (S) and electrical conductivity (σ) of n-doped CNT films stored in (A and B) atmospheric conditions [room temperature (RT)] (air, ~25 °C, 25% to 60% relative humidity) and (C and D) humid conditions (air, ~25 °C, >80% relative humidity): (A and C) TBD-doped and (B and D) 2TBD-C10-doped CNT films. Note that the stability test shown in (D) was started after the initial changes of the TE properties (increase of σ and decrease of $|S|$) had saturated, by first annealing the 2TBD-C10-doped CNT films at 100 °C in air for 1 h.

properties after 3,500 h was markedly restrained (approximately 47% for σ, as compared to the values at approximately 24 h to control for initial changes) compared to those of TBD-doped CNT films incubated for a similar period. Our recent computational calculations revealed that the TBD cation adsorbs onto graphitic carbons with higher energy than that of the acyclic guanidine cation [29]. Holding the 2 TBD parts in a single molecule would allow for rather rigid adsorption of the cation onto the CNT surface at multiple points, contributing to suppressed dopant detachment and the extended stability of 2TBD-C10-doped CNTs.

The power factor of the TBD-doped CNT films exhibited remarkable fluctuation during incubation, as shown in Fig. 4C. Meanwhile, that of the 2TBD-C10-doped CNTs was almost constant during incubation, as shown in Fig. 4D. This was ascribed to the suppressed dedoping, which contributed to ensuring longer-term operation. In summary, 2TBD-C10 doping could induce more thermally stable n-doped states in CNTs compared to TBD doping.

Stability of the doped CNT films in air and under humid conditions

To confirm that thermal energy is one of the origins of partial dedoping of the TBD- or 2TBD-10-treated CNTs (Fig. 4A and B), we proceeded with similar stability tests for the n-doped materials by storing them under atmospheric and humid conditions. The results under atmospheric conditions [air, room temperature (~25 °C), and 25% to 60% relative humidity] are shown in Fig. 5A and B. For the TBD-doped CNT films (Fig. 5A), the electrical conductivity decreased from 1,800 to 1,350 S cm^{-1} (approximately 25% depletion) after storage for 24 h, while the Seebeck coefficient did not show a marked change from the initial value. Additionally, both properties plateaued after 24 h of storage, indicating that less thermal energy from the environment contributes to the extended retention of TE properties.

Meanwhile, the electrical conductivity of the 2TBD-C10-doped CNT films increased up to 2,200 S cm^{-1} after storage under atmospheric conditions for approximately 880 h, as shown in Fig. 5B. A decrease in the absolute value of the Seebeck coefficient was also observed, indicating an increase in electron density because of the progress of doping in the solid state. The slower changes of these properties at room temperature compared to that at 100 °C can be attributed to the lower thermal energy supplied. Therefore, this observation further confirms that the origin of the electron doping progress in the solid state is the structural rearrangement of 2TBD-C10, driven by thermal energy. After the doping progress reached saturation, the TE properties became stable, lasting more than 2,000 h. These retention properties are superior to those of the TBD-doped CNTs. Considering the suppressed dedoping nature at room temperature observed for both TBD- and 2TBD-C10-doped CNTs, thermal energy could be identified as one of the dominant causes of dedoping in these materials.

In addition to thermal energy, humidity is also a potential cause of dedoping; a recent study reported that n-type CNTs created by doping with crown ether complex suffered dedoping because of moisture [38]. Meanwhile, another report suggested that water molecules themselves may contribute to p-type induction in CNTs [39]. The slight depletion of TE properties in TBD-doped CNT films stored at room temperature may thus be attributed to hole injection by naturally adsorbed water molecules in air.

To explore this idea, we investigated the retention of the TE properties under high-humidity conditions (with the relative humidity kept above 80%) at room temperature (approximately 25 °C), as shown in Fig. 5C and D. The depletion of electrical conductivity in the TBD-doped CNTs (approximately 53% decrease after 24 h) was rather remarkable compared to the decreasing trends observed at room temperature without humidity control (Fig. 5A) and even at 100 °C in air (Fig. 4A). However, the Seebeck coefficient of the TBD-doped CNTs hardly changed, as shown in Fig. 5C; we would expect a more remarkable increase in the absolute value of the Seebeck coefficient considering the

Downloaded from https://spj.science.org at Kobe University on September 18, 2024

decrease in conductivity. For instance, we would anticipate an approximate 43% increase in the absolute Seebeck coefficient when the conductivity decreases by approximately 53%, based on the depletion observed at 100 °C in Fig. 4A.

There may be another mechanism at play causing the depletion of TE properties under high humidity conditions, besides the decrease in electron density. Figure S3 demonstrates the recovery of decreased conductivity in TBD-doped CNT films after evacuation following exposure to high-humidity air. The conductivity, which had initially decreased to approximately 760 S cm^{-1}, rebounded to approximately 1,420 S cm^{-1} after evacuation. Therefore, it is reasonable to consider that the predominant mechanism causing the depletion of electrical conductivity under humid conditions is not dedoping (reduction of electron density). Instead, water molecules adsorbed on the CNT surface may act as trap sites for electrons, reducing the carrier mobility [40].

However, such undesired alterations in the TE properties must be avoided for practical applications. A previous study suggested sealing n-doped CNTs with parylene films as moisture-blocking layers [38]; however, it is technologically challenging to uniformly cover the rough surfaces of CNT films. Accidental tearing of the parylene layers can result in water adsorption and depletion of the TE properties of the CNTs. Therefore, ensuring the moisture tolerance of n-doped CNTs themselves is essential.

In this context, 2TBD-C10 offers more feasible n-doped states to CNTs; the 2TBD-C10-doped CNTs retained their properties better than the TBD-doped samples. For example, the decrease in conductivity was only ~24% after 27 h of storage, as shown in Fig. 5D. Although further quantitative analyses are necessary for elucidating the mechanism by which 2TBD-C10 improves the humidity resistance, we hypothesized that the hydrophobic decyl groups in the primary molecular structure of the dopant suppressed the adsorption of water molecules, thereby improving the retention ability under humid conditions. Owing to the enhanced stability of the TE properties, the 2TBD-C10-doped CNT films demonstrated relatively stable power factors during storage in both atmospheric and humid environments, as shown in Fig. S4. The stable TE performance of the 2TBD-C10-doped CNTs, even in elevated-temperature or high-humidity environments, is expected to ensure stable power generation over extended periods.

The morphology of the CNT films hardly changed after 2TBD-C10 doping, as shown in the SEM images in Fig. S5A and B. The diameter of the CNT bundles was comparable before (43 ± 20 nm) and after doping (46 ± 18 nm). Furthermore, the diameter did not change (43 ± 19 nm) after the humidity stability test (Fig. S5C). By contrast, the diameter increased to 73 ± 35 nm after the thermal stability test (Fig. S5D). This is because the supplied thermal energy led to aggregation of the CNTs. The effect of such morphological changes on the stability of the doped states should be addressed in the future. However, the effect is likely to be small because the changes in electrical conductivity and Seebeck coefficient are consistent during incubation (Fig. 4B); this suggests that a trade-off relation exists according to the carrier density rather than the mobility [33]. If the CNT diameter had a more substantial contribution to the carrier mobility, the electrical conductivity would change more drastically than the Seebeck coefficient during incubation.

TE module

To demonstrate the potential of the 2TBD-C10-doped n-type CNT films, we created all-CNT p–n junction TE modules by pairing them with autoxidized p-type films. Before fabricating the modules, we assessed the contact resistance between the p- and n-type CNT films using the transfer length method, employing the geometry outlined in the inset of Fig. 6A. The gap dependence of the electrical resistance (R) between the p-type CNT films is illustrated in Fig. 6A. R was calculated as

$$R = \frac{R_{SH}}{w} L + 2R_c, \quad (3)$$

where R_{SH} denotes the resistance of the films, w denotes the width of n-type CNT films, L denotes the gap between the p-type CNT films, and R_c denotes the contact resistance. Consequently, the intercept on the vertical axis in Fig. 6A is twice the contact resistance ($2R_c$). The contact resistance of the initial p–n junction was approximately 0.3 Ω, with a contact resistivity of 2.7×10^4 μΩ cm^2 based on the contact area of the p–n junction (3 × 3 mm). This value is comparable to the contact resistivity observed between Au and poly(3,3-ethylenedioxithiophene):poly(styrene sulfonate),

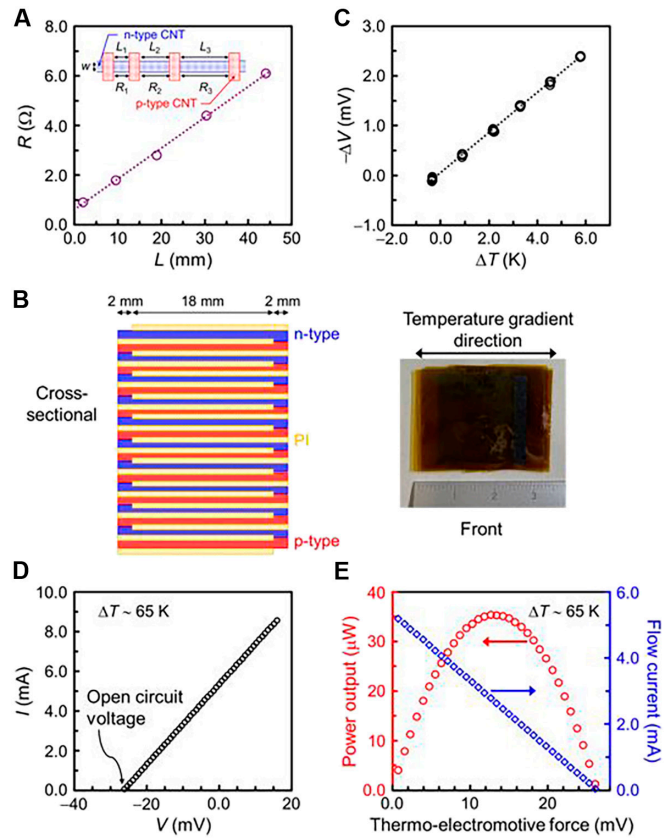

Fig. 6. Fabrication and characterization of all-CNT TE module. (A) Resistance variation according to the gap length between the p-type CNT films. The inset displays a schematic of the geometry for the transfer length method using p- and n-type CNT films. (B) Schematic (cross-sectional view) and photograph (front view) of the all-CNT TE module comprising 10 pairs of p–n units. (C) Plots of thermopower ($-\Delta V$) against the supplied temperature difference (ΔT) of the module measured under open circuit conditions. The temperature difference was supplied in the in-plane direction of the module. (D) Current (I)–applied voltage (V) plots of the module measured while keeping ΔT at approximately 65 K. (E) Power output according to the thermo-electromotive force from the module at ΔT of approximately 65 °C. The plots were created from the data shown in (D).

Downloaded from https://spj.science.org at Kobe University on September 18, 2024

previously utilized in high-performance TE modules [41]. The low contact resistance aids in reducing energy loss at the p–n junctions. Notably, the contact resistivity of the 2TBD-C10-doped n-type CNT film decreased after storage in room temperature air, as depicted in Fig. S6 and Table S3. The contact resistance in organic semiconductors and nanocarbons is related to the carrier density; specifically, increasing the carrier density reduces the contact resistance [42]. This finding supports the advancement of electron injection in the solid state after 2TBD-C10 doping, as demonstrated in Fig. 5B.

In Fig. 6B, we assembled a TE module comprising 10 p–n pairs, where p- and n-type CNT films were alternately stacked with insulating PI films. The module generated approximately 400 μV K^{-1} of thermopower ($-\Delta V$), validated by the $-\Delta V$ versus ΔT plots in Fig. 6C, which confirmed the efficient thermopower addition from each p–n unit. The observed discrepancy between the actual and theoretical values ($-\Delta V$ was expected to be approximately 600 μV K^{-1}, considering the Seebeck coefficient of each material) can be attributed to the presence of p–n junctions in the module, as depicted in Fig. 6B. These areas, with a contact length of 2 mm, did not contribute to the thermopower. Optimizing the contact area will be our focus in future work to maximize the output power and voltage.

We assessed the power output of the module by conducting current (I)–voltage (V) characterization while maintaining a temperature difference (ΔT) of approximately 65 K, as illustrated in Fig. 6D. The open circuit voltage (intercept of the ordinary axis) reached 26 mV. Additionally, we calculated the power output (P) using Eq. 4 for each plot, as shown in Fig. 6E.

$$P = IV. \tag{4}$$

The prepared module achieved a maximum power output of approximately 35 μW with an output voltage of approximately 12.7 mV and a flowing current of approximately 2.8 mA. Considering the cross-sectional area of the module (0.2 × 2.2 cm), the maximum power density reached approximately 80 μW cm^{-2}, marking a noteworthy performance compared to previous all-organic and organic/metal TE modules [10,41,43,44], as shown in Table S4.

Although our modules exhibited an open circuit voltage of only 26 mV, their internal resistance was impressively low at just 5 Ω, evident from the slope of the I–V curve in Fig. 6D. This low resistance is attributed to the high conductivity of the p- and n-type CNT films and their relatively low contact resistivity. Consequently, the output performance of the module is sufficient for driving a DC-to-DC converter with an efficiency exceeding 50%, enabling it to power electric devices effectively [45].

These capabilities were demonstrated by connecting the TE module to a DC-to-DC converter capable of boosting the input voltage from several tens of millivolts to 3 V. The experimental setup is illustrated in Fig. S7A and B. As depicted in Movie S1, the circuit system could repeatedly power a green light-emitting diode. Furthermore, Movie S2 shows that the wireless sensor operated by the circuit could transmit room temperature and humidity sensory data to a smartphone. This transmission was successfully executed 16 times in 10 min, as demonstrated in Fig. S7C.

Discussion

We synthesized a cross-linked organic superbase (2TBD-C10) as a dopant to create n-type CNTs that are resistant to environmental factors. The n-doping mechanism, attributed to the transfer of lone-pair electrons, was confirmed by the solvent-dependent TE properties. Long-term retention tests of the TE properties revealed that the doping progress was facilitated by the thermal energy-assisted structural rearrangement of the dopant within solid CNT films. Doping with 2TBD-C10 resulted in n-type CNTs that are tolerant to air, humidity, and thermal conditions, with better stability than TBD-doped films. This stability can be attributed to the unique molecular structure of 2TBD-C10, facilitating good adsorption on the CNT surfaces, reduced volatility because of the increased molecular weight, and suppressed water adsorption. The stable n-type materials were integrated into all-CNT TE modules, demonstrating good-to-excellent power generation performance with a maximum output power of approximately 35 μW at a temperature difference of 65 K. Overall, our results demonstrate that customizing the primary molecular structures of dopants can enhance the doped states of CNTs, contributing to the advancement of all-CNT TE modules. Future perspectives include optimizing the module structure through thermal and electrical design to maximize the power output.

Acknowledgments

We thank A. Mori, T. Nishino, and R. Nakae for their assistance with NMR, MS, and DSC measurements and synthesis.
Funding: This work was supported in part by the A-STEP program of the Japan Science and Technology Agency (JST) (grant number JPMJTR23R6) and a Grant-in-Aid for Scientific Research (KAKENHI) from the Japan Society for the Promotion of Science (JSPS) (grant number 23K13671).
Author contributions: S.H. and Q.W. conceived the project. M.N. and S.H. prepared the manuscript under the supervision and guidance of Q.W. and Y.K. M.N. carried out the synthesis, film preparation, doping, TE characterization, and spectroscopy. M.N. and Y.K. carried out microscopy. M.N., Q.W., and S.H. performed TE module fabrications and characterizations. All authors contributed to writing the manuscript.
Competing interests: The authors declare that they have no competing interests.

Data Availability

The data that support the findings of this study are available from the corresponding author upon reasonable request.

Supplementary Materials

Figs. S1 to S7
Tables S1 to S4
Movies S1 and S2

References

1. Liu L, Guo X, Lee C. Promoting smart cities into the 5G era with multi-field internet of things (IoT) applications powered with advanced mechanical energy harvesters. *Nano Energy*. 2021;88:106304.
2. Haras M, Skotnicki T. Thermoelectricity for IoT—A review. *Nano Energy*. 2018;54:461–476.
3. Rattner AS, Garimella S. Energy harvesting, reuse and upgrade to reduce primary energy usage in the USA. *Energy*. 2011;36(10):6172–6183.

Downloaded from https://spj.science.org at Kobe University on September 18, 2024

4. Liu W, Kim HS, Jie Q, Ren Z. Importance of high power factor in thermoelectric materials for power generation application: A perspective. *Scr Mater*. 2016;111:3–9.
5. Kim D, Kim Y, Choi K, Grunlan JC, Yu C. Improved thermoelectric behavior of nanotube-filled polymer composites with poly(3,4-ethylenedioxythiophene) poly(styrenesulfonate). *ACS Nano*. 2010;4(1):513–523.
6. Cho C, Stevens B, Hsu J-H, Bureau R, Hagen DA, Regev O, Yu C, Grunlan JC. Completely organic multilayer thin film with thermoelectric power factor rivaling inorganic tellurides. *Adv Mater*. 2015;27(19):2996–3001.
7. Cho C, Wallace KL, Tzeng P, Hsu J-H, Yu C, Grunlan JC. Outstanding low temperature thermoelectric power factor from completely organic thin films enabled by multidimensional conjugated nanomaterials. *Adv Energy Mater*. 2016;6(7):1502168.
8. Chen Y, Zhao Y, Liang Z. Solution processed organic thermoelectrics: Towards flexible thermoelectric modules. *Energy Environ Sci*. 2015;8(2):401–422.
9. Kroon R, Mengistie DA, Kiefer D, Hynynen J, Ryan JD, Yu L, Müller C. Thermoelectric plastics: From design to synthesis, processing and structure–property relationships. *Chem Soc Rev*. 2016;45(22):6147–6164.
10. Bubnova O, Khan ZU, Malti A, Braun S, Fahlman M, Berggren M, Crispin X. Optimization of the thermoelectric figure of merit in the conducting polymer poly(3,4-ethylenedioxythiophene). *Nat Mater*. 2011;10(6):429–433.
11. Patel SN, Chabinyc ML. Anisotropies and the thermoelectric properties of semiconducting polymers. *J Appl Polym Sci*. 2017;134(3):44403.
12. Glaudell AM, Cochran JE, Patel SN, Chabinyc ML. Impact of the doping method on conductivity and thermopower in semiconducting polythiophenes. *Adv Energy Mater*. 2015;5(4):1401072.
13. Dörling B, Ryan JD, Craddock JD, Sorrentino A, El Basaty A, Gomez A, Garriga M, Pereiro E, Anthony JE, Weisenberger MC, et al. Photoinduced p- to n-type switching in thermoelectric polymer-carbon nanotube composites. *Adv Mater*. 2016;28(14):2782–2789.
14. Yamamuro H, Hatsuta N, Wachi M, Takei Y, Takashiri M. Combination of electrodeposition and transfer processes for flexible thin-film thermoelectric generators. *Coatings*. 2018;8(1):22.
15. Sun Y, Sheng P, Di C, Jiao F, Xu W, Qiu D, Zhu D. Organic thermoelectric materials and devices based on *p*- and *n*-type poly(metal 1,1,2,2-ethenetetrathiolate)s. *Adv Mater*. 2012;24(7):932–937.
16. McGrail BT, Sehirlioglu A, Pentzer E. Polymer composites for thermoelectric applications. *Angew Chem Int Ed*. 2015;54(6):1710–1723.
17. Takenobu T, Takano T, Shiraishi M, Murakami Y, Ata M, Kataura H, Achiba Y, Iwasa Y. Stable and controlled amphoteric doping by encapsulation of organic molecules inside carbon nanotubes. *Nat Mater*. 2003;2(10):683–688.
18. Kumanek B, Milowska KZ, Przypis Ł, Stando G, Matuszek K, MacFarlane D, Payne MC, Janas D. Doping engineering of single-walled carbon nanotubes by nitrogen compounds using basicity and alignment. *ACS Appl Mater Interfaces*. 2022;14(22):25861–25877.
19. Hata S, Yamaguchi Y, Nakata R, Kametani K, Du Y, Shiraishi Y, Toshima N. Durable n-type carbon nanotubes double-doped with 1,8-diazabicyclo[5.4.0]undec-7-ene and polyamidoamine dendrimers. *Diam Relat Mater*. 2021;120:108656.
20. Kawasaki K, Harada I, Akaike K, Wei Q, Kosiba Y, Horike S, Ishida K. Complex chemistry of carbon nanotubes toward efficient and stable p-type doping. *Commun Mater*. 2024;5:21.
21. Collins PG, Bradley K, Ishigami M, Zettl A. Extreme oxygen sensitivity of electronic properties of carbon nanotubes. *Science*. 2000;287(5459):1801–1804.
22. McClain D, Thomas N, Youkey S, Schaller R, Jiao J, O'Brien KP. Impact of oxygen adsorption on a population of mass produced carbon nanotube field effect transistors. *Carbon*. 2009;47(6):1493–1500.
23. Lee RS, Kim HJ, Fischer JE, Thess A, Smalley RE. Conductivity enhancement in single-walled carbon nanotube bundles doped with K and Br. *Nature*. 1997;388:255–257.
24. Cho C, Culebras M, Wallace KL, Song Y, Holder K, Hsu J-H, Yu C, Grunlan JC. Stable n-type thermoelectric multilayer thin films with high power factor from carbonaceous nanofillers. *Nano Energy*. 2016;28:426–432.
25. Sarabia-Riquelme R, Craddock J, Morris EA, Eaton D, Andrews R, Anthony J, Weisenberger MC. Simple, low-cost, water-processable *n*-type thermoelectric composite films from multiwall carbon nanotubes in polyvinylpyrrolidone. *Synthetic Met*. 2017;225:86–92.
26. Nonoguchi Y, Ohashi K, Kanazawa R, Ashiba K, Hata K, Nakagawa T, Adachi C, Tanase T, Kawai T. Systematic conversion of single walled carbon nanotubes into n-type thermoelectric materials by molecular dopants. *Sci Rep*. 2013;3:3344.
27. Nonoguchi Y, Nakano M, Murayama T, Hagino H, Hama S, Miyazaki K, Matsubara R, Nakamura M, Kawai T. Simple salt-coordinated n-type nanocarbon materials stable in air. *Adv Funct Mater*. 2016;26(18):3021–3028.
28. Horike S, Wei Q, Akaike K, Kihara K, Mukaida M, Koshiba Y, Ishida K. Bicyclic-ring base doping induces n-type conduction in carbon nanotubes with outstanding thermal stability in air. *Nat Commun*. 2022;13:3517.
29. Nishinaka M, Harada I, Akaike K, Wei Q, Koshiba Y, Horike S, Ishida K. Electrochemical charge-carrier modulation of carbon nanotubes using ionic liquids derived from organic superbases for stable thermoelectric materials. *Carbon*. 2024;218:118667.
30. Persad AH, Ward CA. Expressions for the evaporation and condensation coefficients in the Hertz-Knudsen relation. *Chem Rev*. 2016;116(14):7727–7767.
31. Nakayama H, Schneider JA, Faust M, Wang H, de Alaniz JR, Chabinyc ML. A new family of liquid and solid guanidine-based n-type dopants for solution-processed perovskite solar cells. *Mater Chem Front*. 2020;4(12):3616–3622.
32. Sun P, Wei B, Zhang J, Tomczak JM, Strydom AM, Søndergaard M, Iversen BB, Steglich F. Large Seebeck effect by charge-mobility engineering. *Nat Commun*. 2015;6:7475.
33. Blackburn JL, Ferguson AJ, Cho C, Grunlan JC. Carbon-nanotube-based thermoelectric materials and devices. *Adv Mater*. 2018;30(11):1704386.
34. Freeman DD, Choi K, Yu C. N-type thermoelectric performance of functionalized carbon nanotube-filled polymer composites. *PLOS ONE*. 2012;7(11):e47822.
35. Miller J, Parker AJ. Dipolar aprotic solvents in bimolecular aromatic nucleophilic substitution reactions. *J Am Chem Soc*. 1961;83(1):117–123.
36. Lee S-S, Kim H-S, Hwang T-K, Oh Y-H, Park S-W, Lee S, Lee BS, Chi DY. Efficiency of bulky protic solvent for S_N2 reaction. *Org Lett*. 2008;10(1):61–64.
37. Kim DW, Ahn D-S, Oh Y-H, Lee S, Kil HS, Oh SJ, Lee SJ, Kim JS, Ryu JS, Moon DH, et al. A new class of S_N2 reactions catalyzed

Downloaded from https://spj.science.org at Kobe University on September 18, 2024

by protic solvents: Facile fluorination for isotopic labeling of diagnostic molecules. *J Am Chem Soc*. 2006;128(50):16394–16397.
38. Suzuki D, Nonoguchi Y, Shimamoto K, Terasaki N. Outstanding robust photo- and thermo-electric applications with stabilized n-doped carbon nanotubes by parylene coating. *ACS Appl Mater Interfaces*. 2023;15(7):9873–9882.
39. Hayashi D, Ueda T, Nakai Y, Kyakuno H, Miyata Y, Yamamoto T, Saito T, Hata K, Maniwa Y. Thermoelectric properties of single-wall carbon nanotube films: Effects of diameter and wet environment. *Appl Phys Express*. 2016;9:025102.
40. Kim W, Javey A, Vermesh O, Wang Q, Li Y, Dai H. Hysteresis caused by water molecules in carbon nanotube field-effect transistors. *Nano Lett*. 2003;3(2):193–198.
41. Mukaida M, Kirihara K, Wei Q. Enhanced power output in polymer thermoelectric devices through thermal and electrical impedance matching. *ACS Appl Energy Mater*. 2019;2(10):6973–6978.
42. Matsumoto T, Ou-Yang W, Miyake K, Uemura T, Takeya J. Study of contact resistance of high-mobility organic transistors through comparisons. *Org Electron*. 2013;14(10):2590–2595.
43. Zhou W, Fan Q, Zhang Q, Cai L, Li K, Gu X, Yang F, Zhang N, Wang Y, Liu H, et al. High-performance and compact-designed flexible thermoelectric modules enabled by a reticulate carbon nanotube architecture. *Nat Commun*. 2017;8:14886.
44. Menon AK, Meek O, Eng AJ, Yee SK. Radial thermoelectric generator fabricated from n- and p-type conducting polymers. *J Appl Polym Sci*. 2017;134(3):44060.
45. Mukaida M, Kirihara K, Ebihara T, Wei Q. Gram-scale polymer-based thermoelectric module for charging Li-ion batteries. *Mater Today Energy*. 2023;32:101238.

Downloaded from https://spj.science.org at Kobe University on September 18, 2024